ORIGINAL PAPER

Effect of activation on the carbon fibers from phenol–formaldehyde resins for electrochemical supercapacitors

Rong Xue · Jingwang Yan · Xiaoxue Liu ·
Ying Tian · Baolian Yi

Abstract Activated carbon fibers (ACF) are prepared from phenol–formaldehyde resin fibers through chemical activation and physical activation methods. The chemical activation process consisted of KOH, whereas the physical activation was performed by activation in CO_2. The characteristics of the electrochemical supercapacitors with carbon fibers without activation (CF), carbon fibers activated by CO_2 (ACF-CO_2), and carbon fibers activated by KOH (ACF-KOH) have been compared. The activated carbon fibers from phenol–formaldehyde resins present a broader potential range in aqueous electrolytes than activated carbon and other carbon fibers. Activation does not produce any important change in the shape of starting fibers. However, activation leads to surface roughness and larger surface areas as well as an adapted pore size distribution. The higher surface areas of fibers treated by KOH exhibited higher specific capacitances (214 and 116 F g^{-1} in aqueous and organic electrolytes, respectively) and good rate capability. Results of this study suggest that the activated carbon fiber prepared by chemical activation is a suitable electrode material for high performance electrochemical supercapacitors.

Keywords Carbon fiber · Electrochemical supercapacitors · Phenol–formaldehyde resin · Activation

R. Xue · J. Yan (✉) · X. Liu · Y. Tian · B. Yi
Dalian Institute of Chemical Physics,
Chinese Academy of Sciences, Dalian 116023, China
e-mail: yanjw@dicp.ac.cn

1 Introduction

Electrochemical supercapacitors have recently received much attention in high power electrochemical energy storage technologies due to their high power densities (10 kW kg^{-1}), long cycle lives (10^6 cycles), and safe operation [1]. Activated carbon fibers (ACFs) are promising electrode materials for electrochemical supercapacitors due to its high specific surface area, uniform pore size distribution, and high specific capacity on weight basis [2]. Phenolic resin-based ACFs have been considered as a promising material for the polarizable electrodes of electrochemical supercapacitors with quite large specific surface area, high electrical conductivity, high capacitance, working voltage, reliability, and low leakage current [3].

However, for being effectively used as electrodes for supercapacitors, these materials should fulfill some requirements as an adequate pore size distribution and a large amount of surface functionalities, etc. [1]. Basically, chemical and physical activation of ACFs allow producing materials with certain surface area and pore size distribution [4–7]. In the case of physical activation (H_2O, CO_2, air, etc.), there have been numerous reports regarding the effects of pore structure on capacitor performance [8], which was found to significantly develop pores in a wide range diameters. With regard to chemical activation ($ZnCl_2$, H_3PO_4, KOH, etc.), chemical treatment can affect the electric resistance of ACFC and is used to form micropores [9]. Among the numerous chemical reagents, difference in the chemical activation mechanism, alkali hydroxides were found to be effective in creating the surface oxygen functional groups [10].

Chemical and physical methods of carbon activation are well known and allow producing materials, which influence the final pore size distribution [11]. In this study,

phenol–formaldehyde resin-based carbon fibers (CFs) have been treated by chemical activation of KOH and physical activation of CO_2. The series of electrodes thereof prepared have been electrochemically characterized in aqueous and organic electrolytes. The results show that higher capacitive behavior can be obtained in all electrolytic media for carbon fibers treated by KOH due to larger surface areas and an adapted pore size distribution.

2 Experimental

2.1 Materials

Phenol–formaldehyde resin fibers (Institute of Coal Chemistry, Chinese Academy of Sciences) were used in this study. The fibers were carbonized in a horizontal tubular furnace in N_2 flow of 20 mL min^{-1}. The samples were heated to 850 °C and kept at this temperature for 1 h. The ramps for the heating and cooling steps were set at 2 °C min^{-1}. This carbonized fiber is designated as CF. A commercial activated carbon (YEC-8, Fuzhou Yihuan Co. Ltd., China) was used for comparison. An organic electrolyte, 1 mol L^{-1} solution of tetraethylammonium tetrafluoroborate (TEABF$_4$) in propylene carbonate (PC) was offered by Tianjin Jinniu Power Sources Material Co., Ltd. All chemicals were of analytical grade and used without further purification.

2.2 Chemical activation

Chemical activation of the CFs was conducted by the following procedure: first, CFs were soaked in an aqueous KOH (Shenyang Xinxing Reagent Factory, China) solution at 60 °C overnight and the KOH to CFs mass ratio was 4:1. Activation was carried out in a Ni pan placed in a horizontal tubular furnace in N_2 flow of 20 mL min^{-1}. The samples were heated to 600–900 °C and kept at this temperature for 1 h. The ramps for the heating and cooling steps were set at 2 °C min^{-1}. After cooling, the resulting products were washed consecutively with diluted hydrochloric acid and distilled water until reaching a neutral pH. The samples were finally dried in vacuum at 100 °C for 24 h to obtain chemical activated carbon fibers (denoted as ACF-KOH-T, i.e., ACF-KOH-600, ACF-KOH-700, ACF-KOH-800, and ACF-KOH-900).

2.3 Physical activation

Physical activation of the CFs was carried out in a horizontal tubular furnace in CO_2 flow of 20 mL min^{-1}. The samples were heated to 900 °C and kept at this temperature for 2 h. The ramps for the heating and cooling steps were set at 2 °C min^{-1}. The final products were denoted as ACF-CO$_2$.

2.4 Characterizations of carbon fibers

The specific surface area and pore size distribution of the carbon fibers were determined by N_2 adsorption on a Quantachrome Nova 4000e. Surface morphological images of the activated carbon fibers were taken by a scanning electron microscope (S-800, Hitachi High-Technologies Co., Japan).

2.5 Electrochemical measurements

Electrodes were prepared by the following procedure: The mixture of 85 wt% ACFs, 10 wt% acetylene black (Tianjin Lihua Jin Chemical Co., Ltd., China), and 5 wt% polytetrafluorene ethylene binder (PTFE, Sunrise Power Co., Ltd., China) was pressed into pellets, followed by drying at 60 °C for 12 h. Two- and three-electrode cells were built for different electrochemical investigations. Two-electrode cells were assembled in a 2032 coin cell (Shenzhen Weifeng Electronics Co., Ltd., China). In the aqueous system, grafted polyethylene film separator (Shanghai Shi Long Hi-Tech Co., Ltd., China) and Ni foam current collectors (Changsha Lyrun New Material Co., Ltd., China) were employed. In the organic system, stainless steel current collectors were employed. 6 mol L^{-1} KOH and 1 mol L^{-1} TEABF$_4$/PC were used as electrolytes for the aqueous and organic systems, respectively. The coin cell with the organic electrolyte was assembled in a glove box under Ar atmosphere with H_2O and O_2 levels less than 0.1 ppm. For the three-electrode experiments in KOH media, Ag/AgCl was used as reference electrode and Ni foam was the counter electrode. The cyclic voltammetry (CV) experiments were conducted on a PARSTAT 2273 electrochemical station (Princeton applied research Co., Ltd., USA). The galvanostatic charge–discharge tests were carried out on a battery testing system (BTS50V50 mA, Neware Electronic Co. Ltd.). For the case using the aqueous electrolyte, the cells were charged up to 1.0 V. For the case using organic electrolyte, the cells were charged up to 2.5 V. The current densities were controlled from 50 m to 1 A g^{-1}. Nyquist plots were obtained for the two- and three-electrode cells in the frequency range from 10 mHz to 100 kHz at open circuit voltage by using a PARSTAT 2273 electrochemical station. The amplitude of the applied ac signal was 5 mV.

From the CVs, specific capacitance values are calculated by using the following formula:

$$C = \frac{1}{v(V_c - V_a)} \int_{V_a}^{V_c} I(V) dV$$

where C refers to the specific capacitance (F g^{-1}), v is the potential scan rate (mV s^{-1}), $V_c - V_a$ is the sweep

potential range during discharging and $I(V)$ refers to the response current density (A g^{-1}) [12].

The mass capacitance C_g is dominated by the imaginary part of Nyquist spectra within a sufficiently low frequency range (diffusion control) and the expression can be expressed as

$$C_g(\mathrm{F\,g^{-1}}) = \frac{-1}{2\pi f \times Z_{\mathrm{imag}} \times m}$$

The galvanostatic charge–discharge studies at different temperatures were carried out using the Neware battery testing system. Cell capacitance is deduced from the slope of the discharge curve by:

$$C = \frac{I}{\mathrm{d}V/\mathrm{d}t}$$

where C is cell capacitance in farads (F), I the discharge current in amperes (A), and dV/dt the slope of the discharge curve in volts per second (V s^{-1}). In a symmetrical system, where the active material weight is the same for the two electrodes, the specific capacitance C_{spec} in farads per gram of active material (F g^{-1}) is related to the capacitance of the cell by:

$$C_{\mathrm{spec}} = \frac{2C}{m_{\mathrm{el}}}$$

where m_{el} is the weight (g) of the active material in one electrode.

The samples for electric conductivity measurements were fabricated by pressing a mixture of 90 wt% obtained carbon fibers and 10 wt% binder (PTFE) at 20 MPa. The disk-shaped samples of 13 mm in diameter and approximately 1 mm in thickness were prepared for the tests of electronic conductivity. The electronic conductivity was measured by two-probe DC method.

3 Results and discussion

3.1 Physico-chemical characterization of the activated carbon fibers

SEM images of the carbon fibers, the carbon fibers activated by CO$_2$, and the carbon fibers activated by KOH are shown in Fig. 1a–e. There is no notable shape difference between CFs and activated ACFs. However, the activations lead to significant change in the surface roughness as shown in the insets of Fig. 1. The carbon fibers have a smooth surface (Fig. 1d), whereas the surface of the activated ones became rough (Fig. 1 a–c, e). In addition, highly rugged surfaces are normally observed for the carbon fibers activated by KOH (Fig 1a–c), which was caused by the formation of cavities due to the removal of the impregnated KOH and KOH-derived compounds. A porous structure was developed by

the reaction of K$_2$O with carbon and K intercalation on the surface of carbon fibers [13]. In addition, the gasification of carbon is beneficial for introducing some micropores. The KOH activation mechanism was suggested by Linares-Solano's group as following [14],

$$6KOH + C \rightarrow 3K + K_2CO_3 + 3H_2$$

When increasing the chemical activation temperature, some existing edges and newly created edges were exposed to an attack perpendicular to the basal planes [15, 16]. As a consequence, ACF-KOH-900 has more accessible edges and indentations created by KOH treatment (Fig. 1c), and has rougher surface than ACF-KOH-600 (Fig. 1a) and ACF-KOH-700 (Fig. 1b).

While the CO$_2$ activation only including the following,

$$CO_2 + C \rightarrow 2CO$$

In comparing the chemically activated samples (Fig. 1a–c) with the physically activated one (Fig. 1e), it is clear that KOH corrosion significantly increases the amount of oxygen functional groups [17]. So chemical activation plays an important role in the generation of pseudocapacitance in EDLCs using aqueous electrolytes [20].

The porosity of the carbon fibers, carbon fibers activated by CO$_2$ and KOH, and activated carbon was analyzed by N$_2$ adsorption at 77 K. The N$_2$ adsorption isotherms are shown in Fig. 2; the pore size distribution obtained from these isotherms is presented in Fig. 3; the evolution of the pore volume, Brunauer–Emmett–Teller (BET) and BJH specific surface area are presented in Table 1. According to IUPAC classification, the isotherms of CF, ACF-CO$_2$, ACF-KOH-T, and AC are both type I, characteristic of their microporous features. The pores distributed in the CF, ACF-CO$_2$ ACF-KOH-T, and AC are mainly composed of two groups: micropores and mesopores. Notably, AC, ACF-KOH-T, and ACF-CO$_2$ have a higher value of adsorption than CF. In addition, the volume of micropores is gradually increased following this order: CF < ACF-KOH-600 < ACF-CO$_2$ < ACF-KOH-700 < ACF-KOH-900. According to the t plot model, the micropore area and external surface area of ACF-KOH-T are higher than that of CF and ACF-CO$_2$ when the temperature is higher than 700 °C. The BET specific surface area increases significantly by activation and reaches 1893 m^2 g^{-1} for ACF-KOH-900 and 939 m^2 g^{-1} for ACF-CO$_2$ which is in parallel to the increase of both micropore and mesopore volumes due to the activation of KOH and CO$_2$.

3.2 Electrochemical performance in an aqueous electrolyte

The electrochemical performance of the carbon fibers have been investigated by cyclic voltammograms obtained in

Fig. 1 SEM images of carbon fibers of different activation methods and various activation conditions. **a–c** Carbon fibers activated by KOH at 600, 700 and 900 °C respectively. **d** Carbon fibers activated by CO_2, **e** carbon fibers, and **f** activated carbon. Magnifications of the square regions are shown in the *insets* of **a–e**
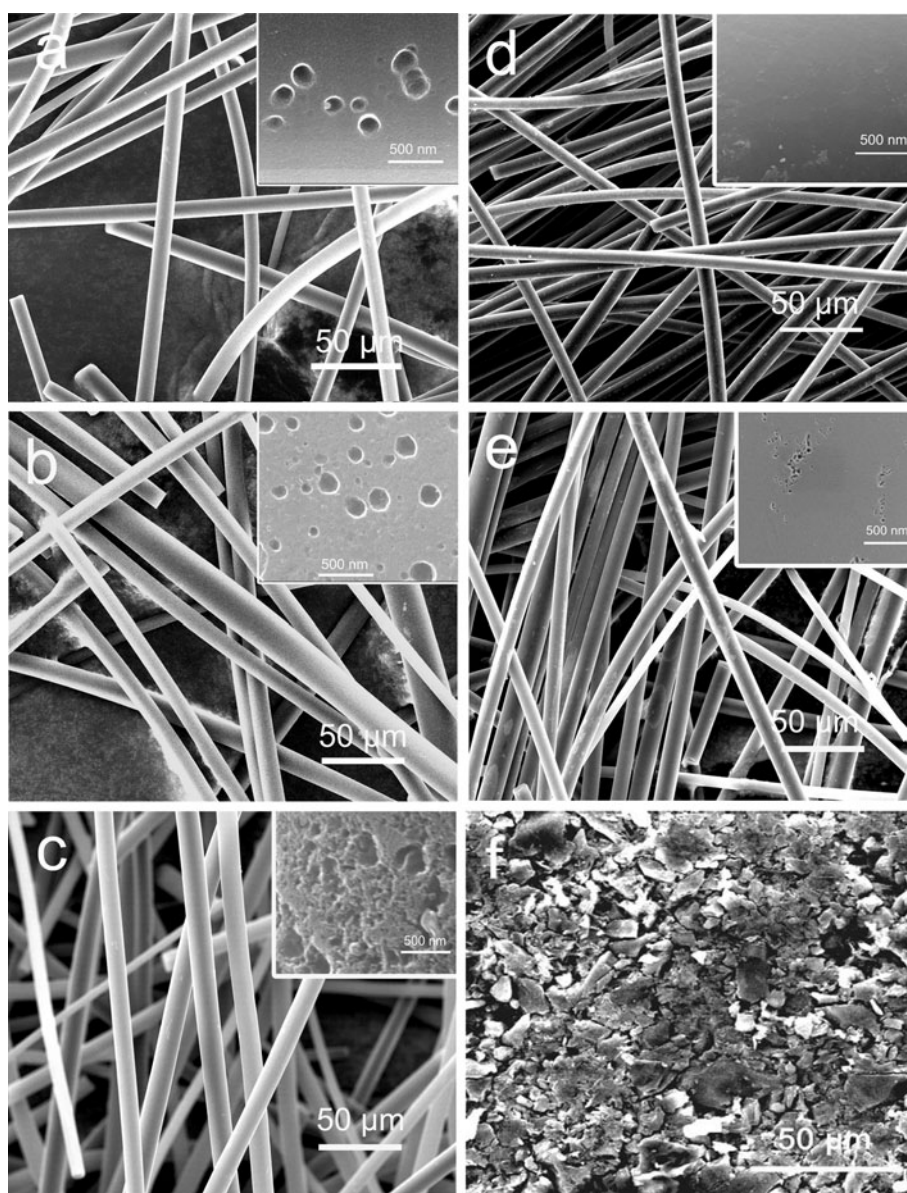
6 mol L^{-1} KOH. Figure 4 shows the CV curves of the ACF-KOH and a commercial activated carbon (AC) at 50 mV s^{-1} in aqueous electrolyte of 6 mol L^{-1} KOH. It seems that the AC is a suitable carbon material for supercapacitor electrode due to its high surface area (Table 1) and the appropriate micropore and mesopore size distribution (Fig. 3c). However, for AC, the anodic current appears at over 0 V versus Ag/AgCl, attributed to oxygen evolution reaction. By contrast, the CV of ACF-KOH presents an almost rectangular shape at 0.2 V versus Ag/AgCl characterizing good capacitive behavior of this material. The shape differences in the CV curves of two materials are attributed to the different morphology of the two materials. As shown in Fig. 1c, the ACF-KOH is highly porous in nature and the interconnected activated carbon fibers allow fast electronic conduction and high

accessibility of the electrolyte in the fabric. But the AC possesses a low uniformity (as shown in Fig. 1f), which can increase the Ohmic resistance of the electrode.

The electrochemical properties of the CF, the CO_2, and KOH-activated carbon fiber electrodes have been investigated in three-electrode cells. Figure 5a shows the cyclic voltammograms obtained for the CF, the CO_2-, and KOH-treated materials in 6 mol L^{-1} KOH. The activated carbon fibers from phenol–formaldehyde resins present no anodic current at high potential and a broader potential range from −1 to 0.2 V in aqueous electrolytes, which is broader than those carbon fibers obtained from Nomex [18] and polacrylonitrile [4, 19]. All samples exhibited nearly rectangular-type *I–V* curves with steep increment in current at the potentials of −1.0 to −0.9 V and this represents the ideal behavior of supercapacitor [1]. The inner integrated area
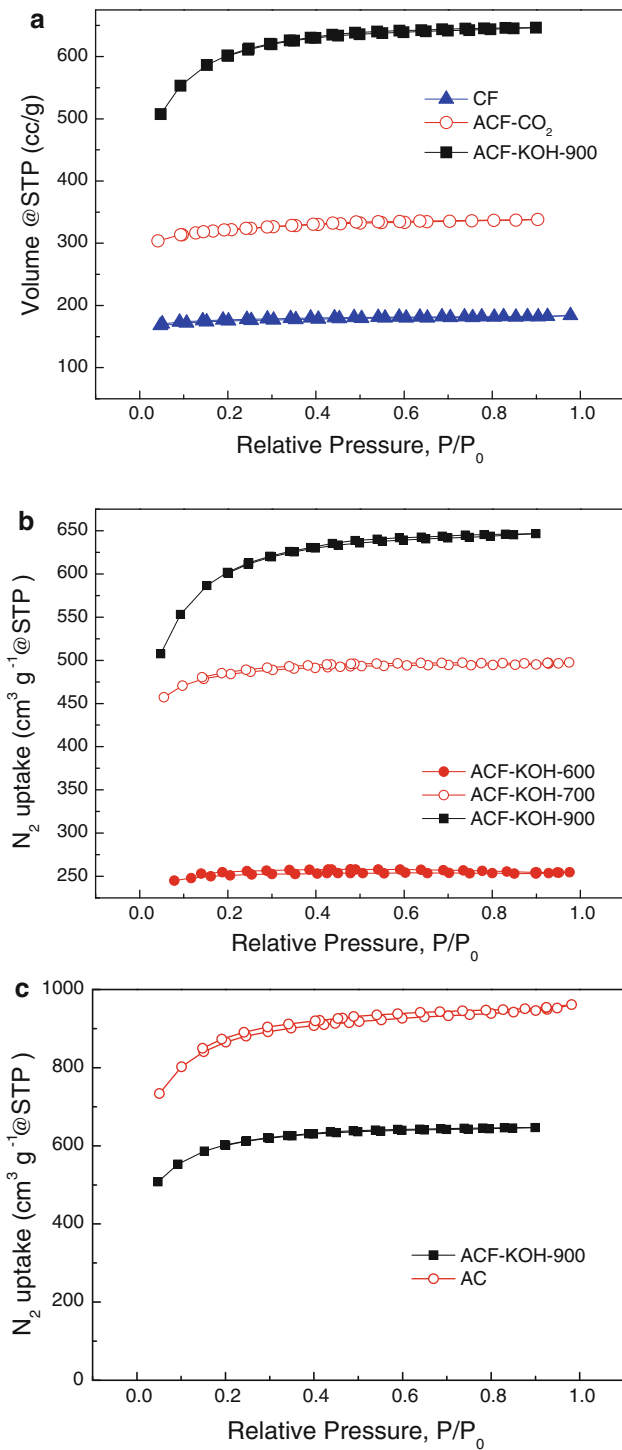
Fig. 2 Curves of nitrogen adsorption isotherms of **a** the phenol–formaldehyde resin and the different activation methods of carbon fiber activated with CO_2 and KOH, **b** carbon fiber activated with KOH at various temperatures, and **c** the carbon fiber activated with KOH and activated carbon
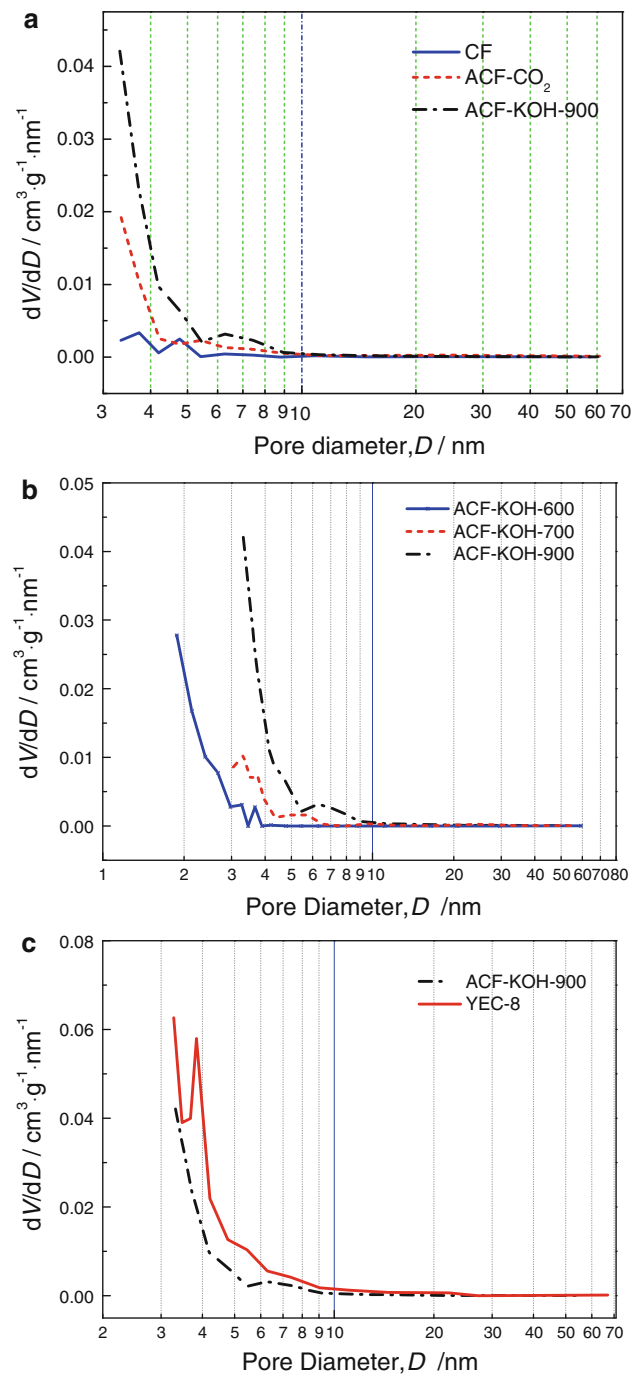

Fig. 3 The pore size distribution obtained from the N_2 desorption data obtained by applying the BJH equation for **a** the phenol–formaldehyde resin and the different carbon fibers activated with CO_2 and KOH, **b** carbon fiber activated with KOH at various temperatures, and **c** the carbon fiber activated with KOH and activated carbon

of CVs, which stands for the power density, increased after the CFs were activated with CO_2 and KOH. From the voltammograms, specific capacitances of the CF, ACF-CO_2,

and ACF-KOH electrodes were evaluated to be 189, 212, and 293 F g^{-1}, respectively. Chemical activation increases the oxygen-containing functional groups on the surface, which play an important role in pseudocapacitance in EDLCs using aqueous electrolytes [20]. Then, the

Table 1 Surface characterization of the carbon fiber (CF) and activated carbon fibers (ACFs)
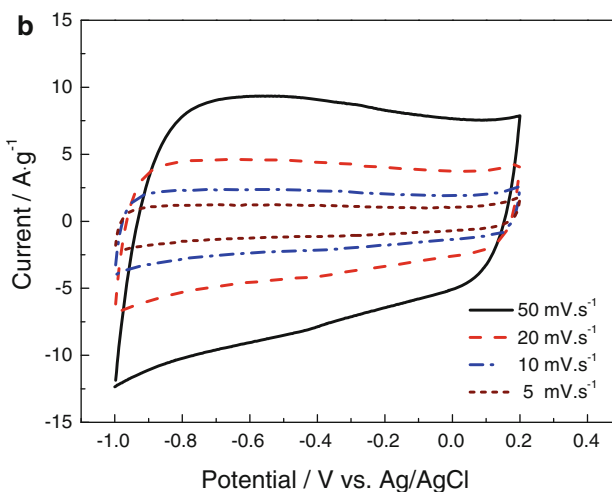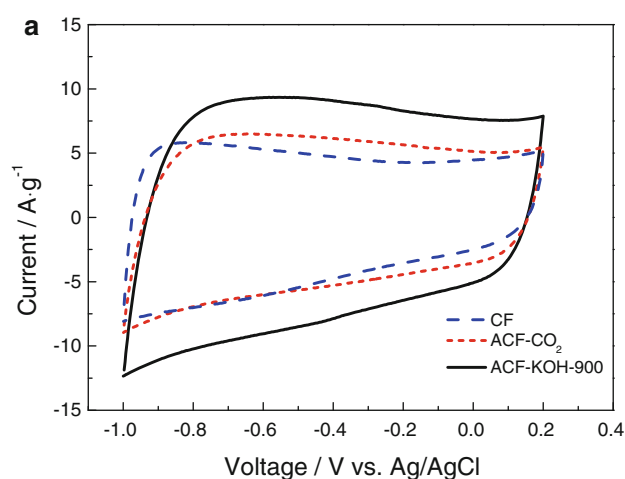
Sample	S_{BET} (m^2 g^{-1})	V_{tot} (cm^3 g^{-1})	V_{mi} (cm^3 g^{-1})	t Plot	
				S_{mi} (m^2 g^{-1})	S_{ext} (m^2 g^{-1})
CF	527.0	0.285	0.250	488.0	39.0
ACF-CO$_2$	939.0	0.534	0.461	858.0	81.2
ACF-KOH-600	738.0	0.390	0.370	709.1	29.3
ACF-KOH-700	1460	0.770	0.690	1350	113
ACF-KOH-900	1893	1.00	0.727	1488	405
AC	2730	1.49	1.04	2130	602

S_{BET} BET surface area, S_{mi} micropore surface area, S_{ext} external surface area, V_{mi} micropore volume, V_{tot} total pore volume
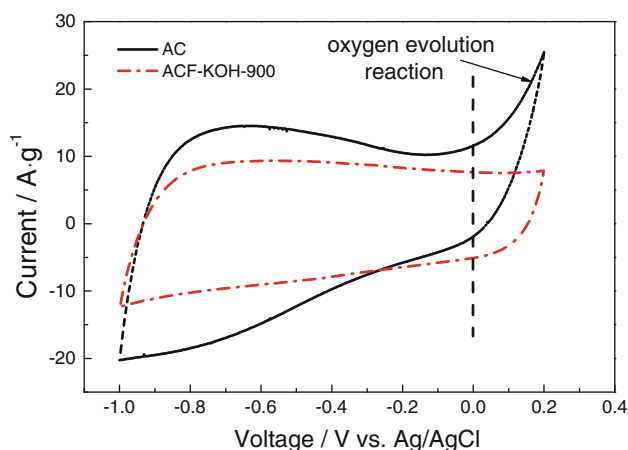
Fig. 4 Three-electrode CV curves of the AC and ACF-KOH-900 at a scan rate of 50 mV s^{-1} in 6 mol L^{-1} KOH

Fig. 5 a Three-electrode CV curves of CFs and ACFs activated by CO$_2$ and KOH at a scan rate of 50 mV s^{-1} in 6 mol L^{-1} KOH; **b** CVs of ACF-KOH-900 in 6 mol L^{-1} KOH at different sweep rates

capacitances of KOH-treated ACFs are higher than the ones obtained by CO$_2$ treatment (Fig. 5a), implying that the surface functionalities on KOH-treated ACFs are more active in aqueous electrolyte. The cyclic voltammetry of the ACF-KOH at different sweep rates was close to the rectangular shape (Fig. 5b). With increasing the sweep rate, the inner integrated area increased, which represented the higher charge/discharge rate and better power density subsequently.

The Nyquist plots for the CFs and the ACFs are shown in Fig. 6a. In the high-frequency region of each spectrum there appears a single semicircle. Following the semicircle with decreasing the frequency, the plots are transformed to a vertical line, which suggest a mainly pure capacitive behavior of the system [21]. The specific capacitances plotted as functions of frequency are shown in Fig. 6b. The capacitance is high at low frequencies for both cases and it starts to decrease at higher frequencies around 0.1–10 Hz. This region corresponds to the transition between the semicircle and the straight line in Fig. 6a. The specific capacitances calculated from Fig. 6b are 124, 128, and 220 F g^{-1} for CF, ACF-CO$_2$, and ACF-KOH, respectively.

Galvanostatic charge–discharge curves for the EDLC cells consisting of CF, ACF-CO$_2$, and ACF-KOH are shown in Fig. 7a. Linear curves were observed in each case. From the galvanostatic charge–discharge curves, at a current density of 50 mA g^{-1}, specific capacitances of the
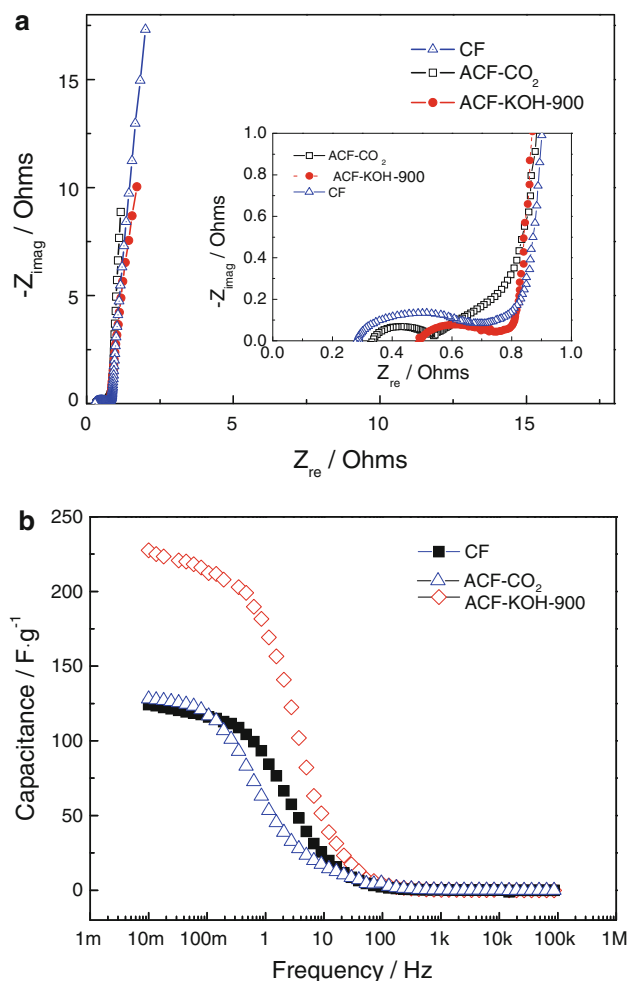
Fig. 6 AC impedance spectra of the CF, CO_2, and KOH-treated ACFs in a 3-electrode system using 6 mol L^{-1} KOH as electrolyte. **a** Nyquist plots (the inset shows the magnification of the semicircle region of the impedance spectra); **b** capacitance versus frequency

Fig. 7 a Charge/discharge curves of the electrodes of CF and ACFs activated with CO_2 and KOH at 50 mA g^{-1} measured in a two-electrode cell using 6 mol L^{-1} KOH as electrolyte and **b** specific capacitances of CF, CO_2-, and KOH-activated ACFs at different current densities

electrodes, CF, ACF-CO_2, and ACF-KOH, were evaluated to be 127, 136, and 214 F g^{-1}, respectively. In addition, the samples showed relatively high rate capability (Fig. 7b).

The dependence of the capacitance of different electrodes derived from ACF-KOH-T on activation temperature is shown in Fig. 8a. It can be seen that the mass capacitance goes through a maximum at moderate activation temperature. Figure 8b presents the mass capacitance values for CF, ACF-CO_2, and ACF-KOH-T samples in the aqueous electrolyte. It is observed that the capacitance increases with the surface area in the aqueous electrolyte. However, the chemically activated one shows higher capacitance than the physically activated ones in aqueous electrolyte, attributing to the existence of the oxygen-containing functional groups on the surface. Moreover, the specific capacitance of the carbon fibers treated by KOH was higher than that of PAN-based ACFs in a KOH medium (ca. 140 F g^{-1}) [19].
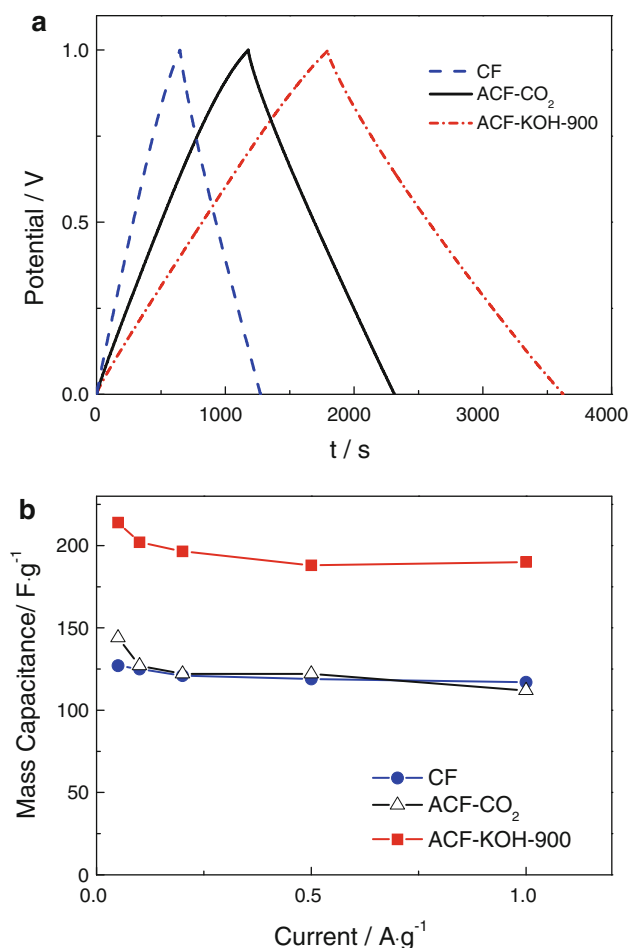
3.3 Electrochemical performance in an organic electrolyte

The electrodes of the CF and carbon fibers activated by CO_2 and KOH have been also assembled in capacitors using an organic electrolyte (TEABF$_4$/PC). The cyclic voltammogram exhibits an almost rectangular shape for ACF-KOH-900, characterizing a good capacitive behavior of this material (Fig. 9a). Different with that for ACF-KOH-900, the CV curves for CF and ACF-CO_2 deviate from a rectangular. Since, the porosity impact the capacitance, the shapes of the CVs between ACF-CO_2 and ACF-KOH-900 is attributed to the differences in pore structure between these two activated ACFs. In addition, the conductivity of the ACF-KOH-900 (12.0 mS cm^{-1}) is higher than that of CF and ACF-CO_2, which is 9.3 and 9.9 mS cm^{-1}, respectively. It demonstrates that both the
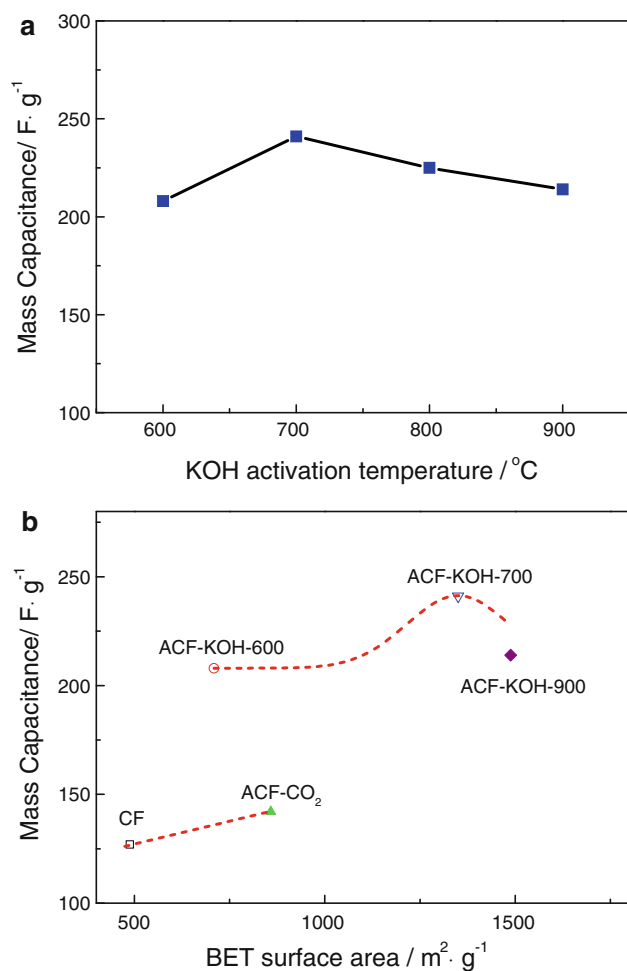
Fig. 8 **a** Temperature on the mass capacitance measured from 2-electrode experiments at a discharge current of 50 mA g^{-1} in 6 mol L^{-1} KOH electrolyte, **b** mass capacitance values versus the BET surface area of the samples for this study at 50 mA g^{-1} in 6 mol L^{-1} KOH electrolyte

Fig. 9 **a** CV curves of the electrode of the CF, CO_2, and KOH-treated carbon fibers at a scan rate of 1 mV s^{-1} in two-electrode cells using organic electrolyte. **b** Charge/discharge curves at 50 mA g^{-1} for a two-electrode cell based on the electrodes of the CF and activated carbon fibers activated with CO_2 and KOH in organic electrolyte

porosity and the electrical conductivity of the carbon fibers account for the distorted CVs.

Figure 9b shows the typical charge–discharge profiles of the CF and ACFs electrodes in the organic electrolyte. Notably, the carbon fibers without activation (CF) present the lower capacitance (18 F g^{-1}) than ACF-CO_2 and ACF-KOH-900 (63 and 116 F g^{-1}, respectively), indicating that the activation process favors the formation and dispersion of pores on the surface of the activated carbon fibers, which increases the specific surface areas and subsequently improves the specific capacitances [22]. The capacitor using ACF-KOH-900 electrodes shows near triangular charge/discharge curves, reflecting its excellent charge/discharge capacitive performance. By contrast, the galvanostatic "voltage–time" curves deviated from linearity for ACF-CO_2. The sharp voltage change at the beginnings of the charge and discharge processes is introduced by the equivalent series resistance (ESR) of the capacitor
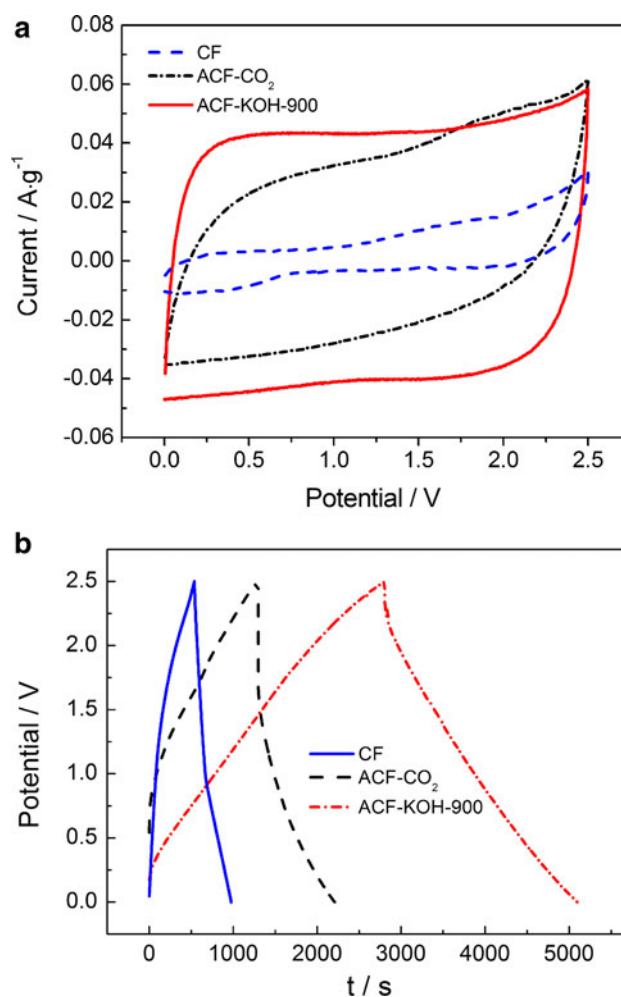
($\Delta V = 2IR$). The ESR is negligible for ACF-KOH capacitor at a current density of 50 mA g^{-1}, demonstrating a high conductivity of the electrodes based on this material. By comparison, the ESR of the ACF-CO_2 capacitor is relative high. The decrease of the sharp drop is attributed to a broader pore size distribution for ACF-KOH-900 (Fig. 3b). As a result, capacitance as high as 116 F g^{-1} can be obtained for the KOH-treated carbon fibers, indicating that the pore size distribution in ACF-KOH is well adapted.

It is noteworthy that the activation temperature has remarkably different effects on the capacitance of the ACF prepared by chemical activation in aqueous and organic electrolytes. Figure 10a shows that the specific capacitance of ACF-KOH-600 is only 10 F g^{-1} at a current density of 50 mA g^{-1}, while it rises up to more than 110 F g^{-1} for ACF-KOH-700. The surface area has substantial
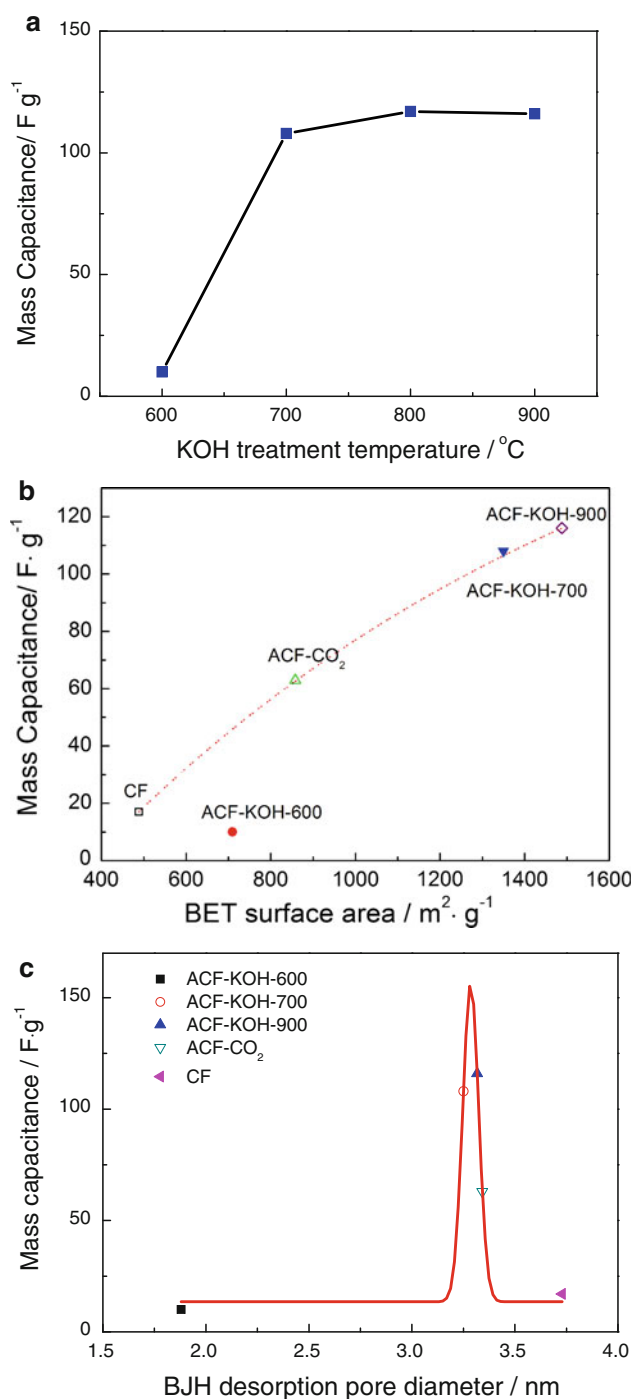
Fig. 10 **a** Temperature effect on the mass capacitance measured from two-electrode experiments at a discharge current of 50 mA g^{-1} in 1 mol L^{-1} $TEABF_4$/PC electrolyte, **b** mass capacitance values versus the BET surface area of the samples at 50 mA g^{-1} in 1 mol L^{-1} $TEABF_4$/PC electrolyte, and **c** mass capacitance as a function of BJH adsorption pore diameter for ACFs at 50 mA g^{-1} in 1 mol L^{-1} $TEABF_4$/PC electrolyte

contribution for the mass capacitances except for ACF-KOH-600 as shown in Fig. 10b. The relationship between the mass capacitance and the BJH desorption pore diameter

(Fig. 10c) shows that the capacitance goes through a maximum at moderate BJH desorption pore diameter. Because, the tetraethylammonium cation and the tetra-fluoroborate anion [23] (0.68 nm vs. 0.33 nm) in the solvent have a structure in which they are surrounded by solvent molecules. Therefore, we can deduce that the diameter of the solvated cation and anion of 3.25 nm is more favorite for the improvement of the specific capacitance.

4 Conclusion

Activated phenol–formaldehyde carbon fibers were prepared by treatment with CO_2 and KOH, respectively. The phenol-resin-based carbon fibers present a broader potential range in aqueous electrolytes than commercial activated carbon. Compared with carbon fibers without activation, specific surface areas increased with the activation of CO_2 and KOH (939 and 1893 m^2 g^{-1}, respectively). The higher surface areas of fibers exhibited higher specific capacitances. Compared with the carbon fibers treated by CO_2, the carbon fibers treated by the ACF-KOH exhibited larger specific surface area, higher capacitance (214 and 116 F g^{-1} in aqueous and organic electrolytes, respectively) and good rate capability. The higher capacitance of ACF-KOH in both electrolytic media is ascribed to the higher surface area and the well-adapted pore size distribution. The pores in ACF-KOH are accessible for the ions with small or large size in different electrolytes. ACF-KOH is a suitable electrode material for high performance electrochemical supercapacitors.

References

1. Conway BE (1999) Electrochemical supercapacitors: scientific fundamentals and technological applications. Kluwer Academic/Plenum Publishers, New York
2. Pandolfo AG, Hollenkamp AF (2006) J Power Sources 157:11
3. Nawa M, Nogami T, Mikawa H (1984) J Electrochem Soc 131:1457
4. Lin JH, Ko TH, Lin YH et al (2009) Energy Fuels 23:4668
5. Xu B, Wu F, Chen RJ et al (2010) J Power Sources 195:2118
6. Ryu ZY, Rong HQ, Zheng JT et al (2002) Carbon 40:1144
7. Barranco V, Lillo-Rodenas MA, Linares-Solano A et al (2010) J Phys Chem C 114:10302
8. Wang KP, Teng HS (2006) Carbon 44:3218
9. Hashisho Z, Rood MJ, Barot S et al (2009) Carbon 47:1814
10. Liu CL, Dong WS, Cao GP et al (2008) J Electrochem Soc 155:F1
11. Braun A, Bartsch M, Schnyder B et al (2002) Carbon 40:375
12. Xie XF, Gao L (2007) Carbon 45:2365
13. Lu CL, Xu SP, Gan YX et al (2005) Carbon 43:2295

14. Lillo-Ródenas MA, Cazorla-Amorós D, Linares-Solano A (2003) Carbon 41:267
15. Kim YJ, Horle Y, Matsuzawa Y et al (2004) Carbon 42:2423
16. Endo M, Lee BJ, Kim YA et al (2003) N J Phys 5
17. Liu CL, Dong WS, Cao GP et al (2007) J Electroanal Chem 611:225
18. Leitner K, Lerf A, Winter M et al (2006) J Power Sources 153:419
19. Kim C, Ngoc BTN, Yang KS et al (2007) Adv Mater (Weinheim, Ger) 19:2341
20. Qiao WM, Yoon SH, Mochida I (2006) Energy Fuels 20:1680
21. De Levie R (1963) Electrochim Acta 8:751
22. Hu JL, Huang JH, Chih Y et al (2009) Diamond Relat Mater 18:511
23. Ue M (1994) J Electrochem Soc 141:3336